Catalysis Science & Technology

Accepted Manuscript

This article can be cited before page numbers have been issued, to do this please use: A. García-Zaragoza, C. Cerezo-Navarrete, A. Mollar-Cuni, P. Oña-Burgos, J. A. Mata, A. Corma and L. M. Martínez-Prieto, *Catal. Sci. Technol.*, 2022, DOI: 10.1039/D1CY02063C.




ROYAL SOCIETY OF CHEMISTRY

rsc.li/catalysis

View Article Online
DOI: 10.1039/D1CY02063C

ARTICLE

# Tailoring graphene-supported Ru nanoparticles by functionalization with pyrene-tagged N-heterocyclic carbenes

Received 00th January 20xx,
Accepted 00th January 20xx

DOI: 10.1039/x0xx00000x

Adrián García-Zaragoza,[a,†] Christian Cerezo-Navarrete,[a,†] Andrés Mollar-Cuni,[b] Pascual Oña-Burgos,[a] Jose A. Mata,[b] Avelino Corma[a] and Luis M. Martínez-Prieto[a,*]

The catalytic properties of graphene-supported ruthenium nanoparticles (Ru@rGO) have been finely tuned by modifying their metal surface with pyrene-tagged *N*-heterocyclic-carbene ligands (pyr-IMes). The nature and interaction modes of the pyr-IMes ligands on Ru@rGO was stablished by XPS, which were found as a protonated carbene, coordinated to the ruthenium surface and directly interacting with the graphene support. To evaluate the activity and selectivity of Ru@GO functionalized with different equivalents of pyr-IMes (Ru@rGO/pyr-IMes$_n$; n= 0, 0.2, 0.5, 0.8 or 1) we used acetophenone hydrogenation as model reaction. The catalytic activity and selectivity are highly dependent on the NHC surface coverage degree. The higher the amount of surface NHC ligands, the lower the activity of the catalyst, but the higher the selectivity towards 1-phenylethanol (supressing the hydrodeoxygenation side-reaction at high surface coverages). The reactivity of the most interesting catalyst, Ru@rGO/pyr-IMes$_{0.5}$, was evaluated in the hydrogenation of other molecules of interest, such as nitrobenzene, 5-hydroxymethylfurfural (HMF), quinoline or 1-methylindole, among others. Finally, by TEM analysis after catalysis we observed a clear correlation between the surface ligand coverage and the stability of the catalysts against sintering. It was then possible to control the reactivity and stability of graphene-supported Ru NPs by modifying their surface with pyr-IMes ligands.

## Introduction

The catalytic use of metal nanoparticles (MNPs) for fine chemical synthesis has undergone an exponential growth since the early 90s.[1] The interest is mainly due to the particular catalytic properties of MNPs, which combine the main advantages of homogeneous and heterogeneous catalysts.[2] Generally, MNPs can be easily recycled and reused as heterogeneous catalysts, but with the characteristic high activity of the homogeneous ones. The high activity of MNPs is explained by their great number of available surface active sites due to their small size (1-100 nm) and high surface-to-volume ratio. However, this large number of surface atoms of different nature normally transforms the reactants in different ways, being difficult to precisely control the selectivity of MNPs. An efficient way to modulate the catalytic performances of MNPs is the use of organic ligands, which can modify the substrate-metal surface interactions during the catalysis and therefore change their activity and selectivity.[3] Controlling the surface chemistry of MNPs by functionalization with ancillary ligands is a well-known strategy in colloidal catalysis.[4] However, it has been much less employed in supported-MNP catalysis, since traditionally it was supposed that surface ligands block active sites decreasing the activity of the supported catalyst, which is a priori an undesired effect.[5] All the same, as well as in organometallic chemistry, surface ligands are also able to modify the electronic and steric properties of supported-MNPs, and thus to modulate their catalytic properties.[6] Thus, the better stability/recyclability of supported-MNPs compared to colloidal MNPs, together with the possibility to control the activity/selectivity through their surface modification with organic ligands, make functionalized supported-MNPs a promising catalyst for industrial processes, since they combine all the benefits of heterogeneous (stability and recyclability) and homogeneous (activity and selectivity) catalysis.

Selective supported metal catalysts are highly important in the industrial synthesis of chemicals.[7] Most industrial catalysts are MNPs supported on high surface area materials that maximizes the metal surface exposure.[8] A strong interaction between the MNPs and the support is crucial to obtain stable catalysts. Moreover, the reactivity of supported-MNPs will not only depend on the particular electronic properties of the metal sites, but also on the chosen support, which, as well as surface ligands, can modify their reactivity.[9] Therefore, the selection of an appropriate support with suitable properties (thermal stability, high surface area, basic/acid sites, etc.) is fundamental for the stabilization of MNPs and to control their catalytic properties. In this line, high surface two-dimensional (2D) structures such as reduced graphene oxides (rGO) are appealing supports for MNPs due to their specific electronic

[a] ITQ, Instituto de Tecnología Química, Universitat Politècnica de València-Consejo Superior de Investigaciones Científicas, Av. de los Naranjos S/N 46022, Valencia, Spain. luismiguel.martinez@csic.es
[b] Institute of Advanced Materials (INAM), Universitat Jaume I, Avda. Sos Baynat S/N 12006, Castellón, Spain.
† These authors contributed equally to this work.
Electronic Supplementary Information (ESI) available: [details of any supplementary information available should be included here]. See DOI: 10.1039/x0xx00000x

configuration that results in strong MNP-graphene interactions.[10] As already mentioned, these metal-graphene interactions can also modify the electronic properties of the supported-MNPs, changing their reactivity.[11] In addition, the defect sites normally present in rGO are excellent anchoring points for MNPs, facilitating their generation and stabilization.[12] All this, together with the recent advances in the synthesis of graphene materials, make graphene-supported MNPs an attractive heterogeneous catalyst for industrial applications.

Since the isolation of the first example of an *N*-heterocyclic carbene (NHC),[13] this type of compounds have been extensively used as ancillary ligands in coordination chemistry.[14] Due to their excellent electron donating properties, NHC ligands strongly coordinate to transition metals, being exceptional ligands for transition metal complexes.[15] However, they are not only suitable ligands for the stabilization of organometallic complexes, but also they are effective MNP stabilizers.[16] Indeed, during the last decade a great number of NHC-stabilized MNPs have been reported, including Au,[17] Ir,[18] Ru,[19] Ni,[20] Pd,[21] or Pt[22] NPs. Moreover, NHCs have demonstrated to be an efficient tool to modify the size, stability, solubility and catalytic properties of MNPs. Depending on the molecular structure (e.g. backbone with long alkyl chains) or N-substituents (e.g. bulky groups) of the stabilizing NHC, the resulting MNPs will display different properties.[16,23] Thanks to their versatility, NHC-stabilized MNPs have been successfully applied in numerous catalytic processes such as hydroboration,[24] oxidation,[23c] deuteration[25] and hydrogenation reactions.[26] In the same way that NHCs can modify the catalytic properties of colloidal MNPs, they can be also used to functionalize supported-MNPs and thereby modulate their surface chemistry.[27] For example, in 2016, Glorius *et al.* have reported how to control the selectivity of Ru/K-$Al_2O_3$ by functionalization with NHCs in the hydrogenation of phenylacetylene to ethylbenzene.[28] Pieters *et al.* have also controlled the selectivity of Ru NPs supported on carbon in the isotopic H/D exchange by modifying the surface metal with NHCs.[29] However, the surface modification of supported-MNPs with NHCs not only may improve their selectivity, but also is able to increase their stability. Recently, it has been shown that NHCs bearing a pyrene group can enhance the stability of graphene-supported MNPs via non-covalent π-interactions between the pyrene tag and the graphene layer.[30]

Herein, we present Ru NPs supported on reduced graphene oxide (**Ru@rGO**) functionalized with different equivalents (0.2, 0.5, 0.8 and 1 equiv.) of an NHC ligand containing a pyrene group (pyr-IMes). The obtained catalytic systems (**Ru@rGO/pyr-IMes**) have been fully characterized by state-of-the-art techniques. Additionally, it has been possible to modify their stability, activity and selectivity in the hydrogenation of different substrates (*i.e.* acetophenone, decanal, nitrobenzene, styrene, 3-methyl-2-cyclohexenone, quinoline, 1-methylindole and HMF) by means of the NHC surface coverage.

## Results and discussion

**Synthesis, characterization and surface studies.**

Ruthenium nanoparticles onto rGO (**Ru@rGO**) functionalized with NHC ligands containing a pyrene tag were prepared following a two-step synthetic route (Figure 1). First, (i) Ru NPs were generated through an organometallic approach and directly immobilized onto reduced graphene oxide (rGO). More specifically, graphene supported Ru NPs (**Ru@rGO**) were generated by the controlled decomposition of Ru(COD)(COT) (COD: cyclooctadiene; COT: cyclooctatriene) under 3 bar $H_2$ in a THF dispersion of rGO, according to previously reported procedure.[31] Then, (ii) the as-synthesized **Ru@rGO** was functionalized with different amounts of a pyrene-tagged *N*-heterocyclic carbene ligand (n = 0.2, 0.5, 0.8 or 1 equivalents relative to ruthenium),[32] formed by the deprotonation of the corresponding imidazolium salt with K*t*BuO. Purification by washing with THF yields Ru NPs immobilized onto rGO functionalized with NHC ligands as black powders, namely **Ru@rGO/pyr-IMes$_n$**.

Ruthenium contents in **Ru@rGO** and **Ru@rGO/pyr-IMes$_n$** were determined by inductively coupled plasma optic emission spectroscopy (ICP-OES) analysis employing an optimized digestion method.[31] In all cases, the ruthenium content was close to the theoretical value of 3 wt% (for more details see Experimental Section).

View Article Online
DOI: 10.1039/D1CY02067G

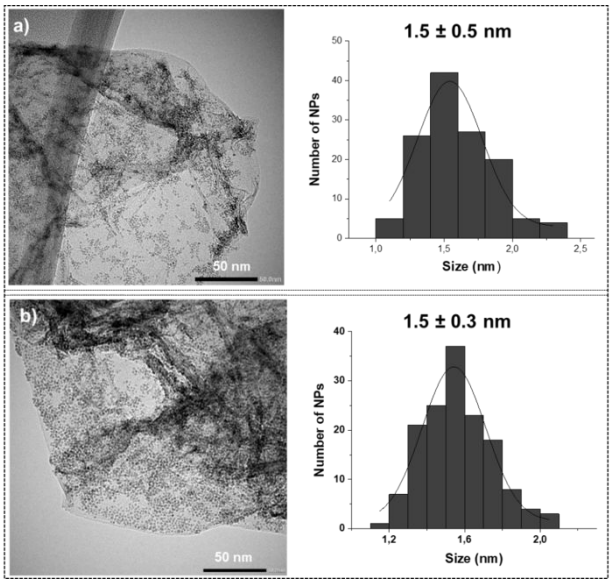


**Figure 2.** Comparative TEM images and size distribution histograms of (a) **Ru@rGO** and (b) **Ru@rGO/pyr-IMes$_{0.5}$**.

Transmission electron microscopy (TEM) analysis of the unmodified **Ru@rGO** revealed the presence of small spherical Ru NPs displaying low dispersion in size, good distribution on the graphene-support and a mean diameter of 1.5 ± 0.5 nm (Figure 2a). After their functionalization with 0.2, 0.5, 0.8 or 1 equivalents (equiv.) of pyr-IMes (**Ru@rGO/pyr-IMes$_n$**) the morphology, size, dispersion and distribution of the graphene-supported Ru NPs did not significantly change (Figure 2b; see ESI, Figures S1-3). A high-resolution TEM (HRTEM) micrograph of **Ru@rGO** (Figure S4) indicates the presence of crystalline nanoparticles with the hexagonal close-packed (hcp) structure characteristic of bulk Ru(0). Fourier transform analysis applied to this picture shows reflection planes at (102), (002) and (101). Since Raman spectroscopy is an established tool to investigate the quality of graphenic materials (defects, exfoliation degree, $sp^2$ character, etc.), **rGO**, **Ru@rGO** and **Ru@rGO/pyr-IMes$_{0.5}$** were analyzed by this spectroscopic technique. In all recorded Raman spectra two well-differenced domains were observed, one located between 1200 and 1700 $cm^{-1}$ and another one from 2500 to 3250 $cm^{-1}$ (see ESI, Figure S5-S7). The first domain contains two bands of similar intensities at 1354 and 1595 $cm^{-1}$, which correspond to D and G bands, respectively. The high ratio of the intensities of these bands ($I_D/I_G$) is related to a high percentage of defect sites, which are normally excellent anchoring points for MNP stabilization.[12,33] In addition, comparing the $I_D/I_G$ ratio before (rGO; Figure S5) and after the incorporation of Ru NPs (**Ru@rGO** or **Ru@rGO/pyr-IMes$_{0.5}$**; Figures S6 and S7), a slight decrease from 1.54 to 1.50 was observed. This decrease in the $I_D/I_G$ ratio is an indication of the increase of the $sp^2$ character of **Ru@rGO** and **Ru@rGO/pyr-IMes$_{(0.5)}$**, mainly due to the incorporation of Ru NPs. The second domain centered at ca. 3000 $cm^{-1}$ corresponds to the 2D band and is related to few graphene layers.

A series of surface studies were performed in order to better understand the coordination mode, location and dynamics of the pyrene-tagged *N*-heterocyclic carbenes at the MNP surface. First, to estimate the precise amount of pyr-IMes ligand incorporated into each one of the functionalized catalysts, a combined study involving elemental analysis (EA) and BET surface area determination was carried out. Once the available surface area of **Ru@rGO** was determined (331.8 $m^2/g$), we calculated by EA the real amount of pyr-IMes ligand added on **rGO**, and thus the actual number of equivalents of pyrene-tagged NHCs with which each catalyst has been functionalized (Table S1). As general trend, only half of the amount of NHC ligand added during the synthesis was finally incorporated to the functionalized catalysts.

Subsequently, a CO chemisorption analysis was performed to determine the accessible ruthenium surface of the unmodified **Ru@rGO** and the functionalized **Ru@rGO/pyr-IMes$_{0.5}$**, and therefore, to evidence the coordination of the carbene ligand to the ruthenium surface. For the unmodified **Ru@rGO**, the CO uptake was 62.1 $\mu g/g^{-1}$, while for **Ru@rGO/pyr-IMes$_{0.5}$** the uptake of CO decreases to 35.9 $\mu g/g^{-1}$. The decrease in the number of available Ru sites on **Ru@rGO/pyr-IMes$_{0.5}$** is attributed to the coordination of pyr-IMes on the Ru surface, which blocks potential CO adsorption sites. Therefore, this partial decrease in the chemisorption of CO not only confirms the coordination of pyr-IMes to Ru NPs, but also demonstrates the presence of available active surface sites on the functionalized catalysts. With the aim to shed some light in the nature and location of these active sites, and to further investigate the coordination of pyr-IMes at the Ru surface, the unmodified and functionalized graphene-supported Ru NPs were studied by IR and solid-state MAS-NMR spectroscopies

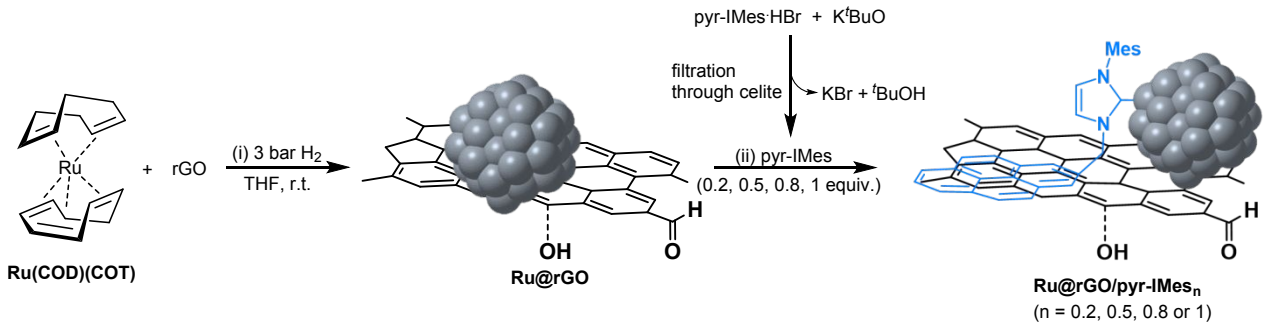


**Figure 1.** Two-step synthetic route followed for the synthesis and subsequent functionalization of **Ru@rGO** with pyr-IMes.

using CO as a probe molecule. However, due to their opacity and conductivity (which made impossible the tuning of the NMR probe), these analyses were unsuccessful. To circumvent this limitation, colloidal/unsupported Ru NPs stabilized with 0.2 and 0.5 equiv. of pyr-IMes (**Ru/pyr-IMes$_{0.2}$** and **Ru/pyr-IMes$_{0.5}$**) were synthesized and fully characterized, including IR and MAS-NMR surface studies using CO as molecular probe. NHC ligand-stabilized Ru NPs were prepared following the same organometallic approach illustrated in Figure 1, but using the pyrene-tagged NHC ligands as stabilizer (Figure 3). Here, the non-supported Ru NPs are directly stabilized by the NHC ligands, as it has been previously described.[23b]

TEM and HRTEM images of **Ru/pyr-IMes$_{0.2}$** and **Ru/pyr-IMes$_{0.5}$** showed small, crystalline and monodispersed Ru NPs with a mean diameter of 1.4 ± 0.4 and 1.3 ± 0.4 nm, respectively (see ESI, Figures S8, S9 and S10). ICP analyses of **Ru/pyr-IMes$_{0.2}$** and **Ru/pyr-IMes$_{0.5}$** gave ruthenium contents of 55.7 and 33.2 wt%, respectively. It is worth to mention that the ratio between surface ruthenium atoms and coordinated NHC ligands ($Ru_{(s)x}/L_y$) is not large enough to accommodate all the ligands on the Ru surface (steric hindrance). More specifically, **Ru/pyr-IMes$_{0.2}$** exhibits a $Ru_{(s)x}/L_y$ ratio of *ca.* 4.1**,** while the ratio for **Ru/pyr-IMes$_{0.5}$** is even lower, 1.4 (see ESI, Table S2). Therefore, we can assume that the remaining surface ligands are organized in a second coordination sphere by π–π stacking between the aromatic side groups of the pyrene-tagged NHCs. This type of second sphere of non-coordinated ligands have been previously observed in similar ligand-stabilized MNPs.[22,34]

Afterwards, the surface state of **Ru/pyr-IMes$_{0.2}$** and **Ru/pyr-IMes$_{0.5}$** was investigated by evaluating their capacity to bind CO by diffuse reflectance infrared Fourier transform (DRIFT) and $^{13}C\{^1H\}$ MAS NMR with $^1H$–$^{13}C$ cross-polarization (CP). Here the aim was to locate the available surface active sites of these NHC-stabilized Ru NPs. Figures S11 and S12 (see ESI) show DRIFT spectra of **Ru/pyr-IMes$_{0.2}$** and **Ru/pyr-IMes$_{0.5}$** before (blue) and after (red) exposure to CO (bubbling CO in a THF solution, for more details see Experimental Section). Interestingly, before reaction with CO, both spectra already exhibited a weak and broad band at *ca.* 1900 $cm^{-1}$, corresponding to adsorbed CO. The presence of this band is attributed to the decarbonylation of THF during the synthesis of the nanoparticles, as previously observed.[23c,35] After reaction with CO, both spectra showed an increase in intensity and a shift to higher frequency (*ca.* 2000 $cm^{-1}$) of the aforementioned band. This confirmed the coordination of CO and the existence of a high availability of free Ru active sites at the NP surface, even in the presence of a large number of surface NHC ligands, as was previously determined by ICP (see ESI, Table S2).

$^{13}C\{^1H\}$ CP-MAS NMR spectrum of **Ru/pyr-IMes$_{0.2}$** displayed a number of distinct peaks characteristic of the pyrene-tagged NHC ligand (see ESI, Figure S13a). The broad signal at *ca.* 130 ppm was assigned to the aromatic rings of the mesitylene and pyrene groups, together with the imidazole backbone. The peaks between 50 and 10 ppm were attributed to the $CH_2$ group connected to the pyrene tag, as well as the methyl groups of the N-bonded mesitylene. After expose **Ru/pyr-IMes$_{0.2}$** NPs to 1 bar of $^{13}CO$ at room temperature (r.t.), the $^{13}C\{^1H\}$ CP-MAS NMR spectrum showed two new signals ascribed to adsorbed CO (Figure S13b). A broad and low-intensity resonance at *ca.* 230 ppm corresponding to $^{13}CO$ coordinated in a bridging mode ($CO_b$), and a sharp and intense peak at ca. 200 ppm due to $^{13}CO$ adsorbed in a terminal mode ($CO_t$). It is well know that bridging CO molecules coordinate onto nanoparticle faces (or terraces) and terminal ones onto their apexes and edges.[36] Since most of CO coordinates in a terminal mode, we can assume that ruthenium faces are not accessible due to the π interactions between the aromatic rings of the pyrene and the ruthenium terraces, which hinder the coordination of CO in bridging mode.[37] Furthermore, the appearance of spinning side bands (*) suggests that terminal COs statics on the surface. This lack of mobility of $CO_t$ on the ruthenium surface can be explained by the coordination of NHC ligands near to the active sites where CO molecules are adsorbed. $^{13}C\{^1H\}$ CP-MAS NMR spectrum of **Ru/pyr-IMes$_{0.5}$** after exposure to $^{13}CO$ showed similar resonances, but with a new peak at 204 ppm (see ESI, Figure S14). This new resonance may correspond to the CO coordinated in a multi-terminal mode, as previously reported for Rh NPs.[38] Again, we observed by CP-MAS NMR a great number of free active sites on these non-supported Ru NPs even at high surface ligand coverages

The coordination of pyr-IMes on the non-supported **Ru/pyr-IMes$_{0.5}$** NPs was also investigated by X-ray Photoelectron Spectroscopy (XPS), since it is a useful tool to study the binding mode of NHC surface ligands on MNPs.[39] The N 1s area of **Ru/pyr-IMes$_{0.5}$** presents a binding energy (BE) of 399.1 eV (Figure 4a, orange), which is shifted to low BE values compared

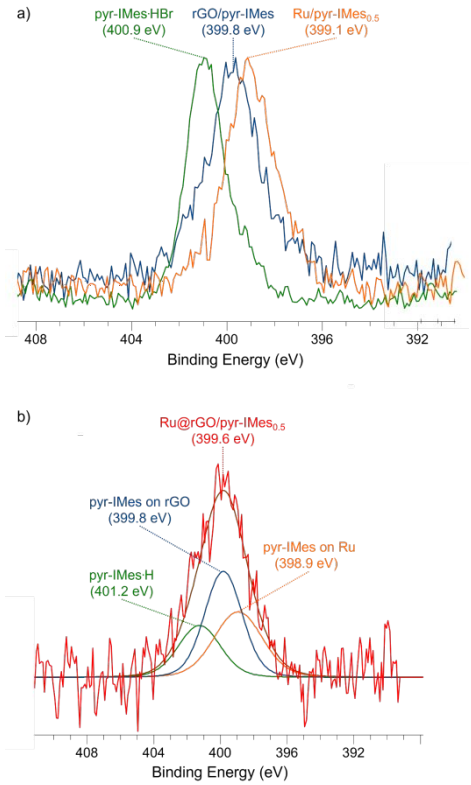


**Figure 4.** X-ray photoelectron spectroscopy (XPS) of (a) the N 1s signals of pyr-IMes·HBr (green), **rGO/pyr-IMes** (blue), **Ru/pyr-IMes$_{0.5}$** (orange) and (b) **Ru@rGO/pyr-IMes$_{0.5}$** (red).

to the corresponding imidazolium salt **pyr-IMes·HBr** (400.9 eV) (Figure 4a, green). This decrease in the BE is due to a loss of electron density of the N atoms of Pyr-IMes and indicates the direct coordination of the NHC ligand to the ruthenium surface. XPS analysis was also employed to investigate the coordination of the pyrene-tagged NHC ligand on the graphene-supported Ru NPs functionalized with 0.5 equivalents of pyr-IMes (**Ru@rGO/pyr-IMes$_{0.5}$**). For **Ru@rGO/pyr-IMes$_{0.5}$** the N 1s peak is centered at 399.6 eV, and can be deconvoluted in three contributions with different BEs (Figure 4b), corresponding to pyr-IMes coordinated to Ru (398.9 eV), interacting with rGO (399.8 eV), and protonated (401.2 eV). To confirm the BE of pyr-IMes which is directly interacting with the rGO support (**rGO/pyr-IMes**), most probably by π-interactions between the pyrene tags of the NHC and the graphene layer, free NHC was added to a dispersion of rGO in THF and analyzed by XPS (for more details see Experimental section). And, as was expected, the N 1s signal of **rGO/pyr-IMes** revealed a peak at 399.8 eV, which is located between the N 1s peaks of the corresponding imidazolium salt and the pyr-IMes ligand coordinated to ruthenium (Figure 4a, blue). Therefore, using XPS we were able to evaluate the different nature and chemical environments of pyr-IMes ligands on the functionalized catalyst, **Ru@rGO/pyr-IMes$_{0.5}$**: (i) protonated (400.9 eV), (ii) coordinated to ruthenium (399.1 eV) and (iii) interacting with the graphene support (399.8 eV) (Figure 4.) Furthermore, by analyzing their N 1s XPS areas after deconvolution, we can deduce that approximately 32 % of the NHC ligand is coordinated to Ru, 45 % is interacting with the graphene support and 23 % is protonated.

Moreover, the oxidation state of the ruthenium was also investigated by XPS upon analyzing the Ru 3p region of **Ru/pyr-IMes$_{0.5}$**, **Ru@rGO** and **Ru@rGO/pyr-IMes$_{0.5}$** (Figure S15). The Ru 3p$_{3/2}$ signal of the ligand-stabilized **Ru/pyr-IMes$_{0.5}$** was found at 462.2 eV, which after deconvolution showed two contributions, a main contribution at *ca.* 461.4 eV, attributed to Ru(0), and a minor one at *ca.* 463.8 eV corresponding to $RuO_2$ (Figure S15a). On the other hand, Ru 3p$_{3/2}$ signals of graphene-supported Ru NPs unmodified and modified with pyr-IMes were observed at 463.1 and 463.4 eV, respectively (see ESI, Figures S15b and S15c). After deconvolution, we observed that most of the ruthenium was oxidized to Ru(IV). This is mainly due to the purification process of the graphene-supported Ru NPs, which is carried out under air (see Experimental Section). For this reason, a preliminary activation step (1 h at 150 °C and 50 bar $H_2$) was necessary before catalysis. This activation step reduces most of $RuO_2$ to Ru(0), which is the active species in hydrogenation reactions.

**Catalytic studies.**

First, to evaluate the influence of the pyrene-tagged NHC ligands on the activity and selectivity of the graphene-supported Ru NPs, the hydrogenation of acetophenone was

**Table 1.** Hydrogenation of acetophenone catalyzed by **Ru@rGO/pyr-IMes$_n$** (X = 0.2, 0.5, 0.8 or 1) and **Ru@rGO/ICy$_1$**.[a]

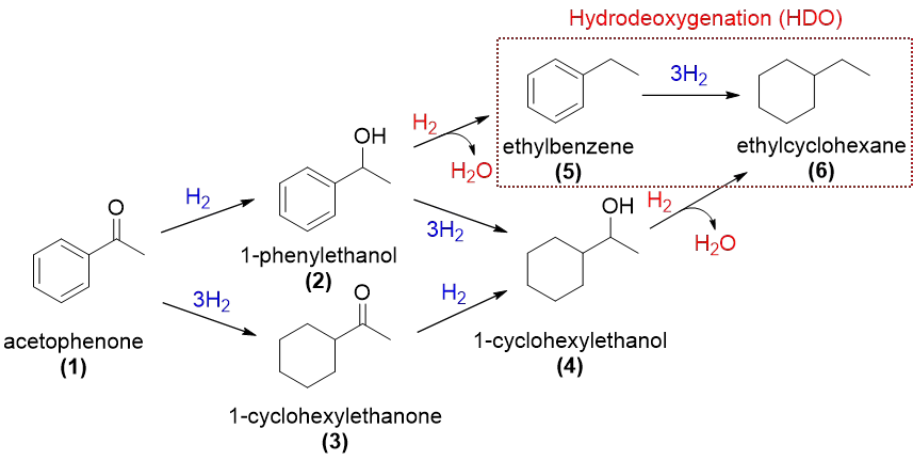


| Entry | Catalyst | Conversion (%)[b,c] | Selectivity (%)[b] 2 | 3 | 4 | 5 | 6 |
|---|---|---|---|---|---|---|---|
| 1 | **Ru@rGO** | > 99 | 0.0 | 0.0 | 81.5 | 0.0 | 18.5 |
| 2 | **Ru@rGO/pyr-IMes$_{0.2}$** | > 99 | 1.1 | 8.7 | 69.6 | 3.9 | 16.7 |
| 3 | **Ru@rGO/pyr-IMes$_{0.5}$** | 98.6 | 1.9 | 5.0 | 84.1 | 0.1 | 8.9 |
| 4 | **Ru@rGO/pyr-IMes$_{0.8}$** | 95.9 | 63.6 | 9.8 | 21.7 | 4.2 | 0.7 |
| 5 | **Ru@rGO/pyr-IMes$_1$** | 60.2 | 98.0 | 0.8 | 0.6 | 0.6 | 0.0 |
| 6 | **Ru@rGO/ICy$_1$** | 98.4 | 0.0 | 9.6 | 77.2 | 3.7 | 9.5 |

[a] Reaction conditions: 0.5 mmol acetophenone, 0.5 mol% cat. (0.0025 mmol Ru), 10 mL THF, 50 bar H2, 130 ºC, 20h.

[b] Conversions and selectivities were determined by GC using dodecane as internal standard, and confirmed by GC-MS.

[c] Metal-free rGO exhibited negligible activity in the hydrogenation of acetophenone under these reaction conditions.

View Article Online
DOI: 10.1039/D1CY02063C



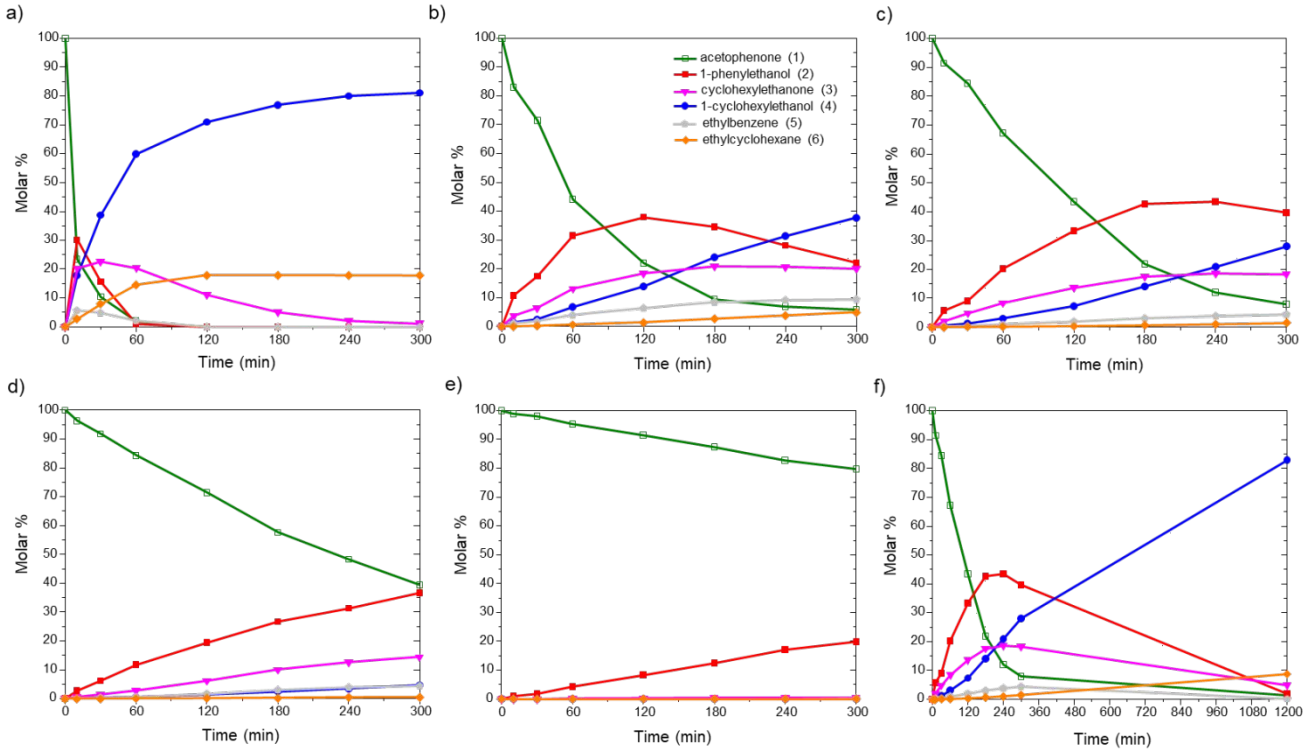


**Figure 5.** Hydrogenation of acetophenone using (a) **Ru@rGO**, (b) **Ru@rGO/pyr-IMes$_{0.2}$**, (c and f) **Ru@rGO/pyr-IMes$_{0.5}$**, (d) **Ru@rGO/pyr-IMes$_{0.8}$**, and (e) **Ru@rGO/pyr-IMes$_{1}$** as catalysts.

used as a model reaction. This substrate is an interesting model molecule since it contains two potentially reducible functional groups (*i.e.* a ketone and a phenyl group), and the activity/selectivity of the functionalized catalysts herein prepared can be simply compared. Acetophenone (**1**) can be reduced to 1-cyclohexylethanol (**4**) through two pathways: (i) via 1-phenylethanol (**2**), hydrogenating first the ketone, and (ii) via 1-cyclohexylethanone (**3**), where the phenyl group is hydrogenated before (top of Table 1). Additionally, ethylbenzene (**5**) and ethylcyclohexane (**6**) can be also formed by hydrodeoxygenation (HDO) processes. By checking the selectivity of the non-functionalized **Ru@rGO** at total conversion (20h, Table 1, entry 1), it can be seen that it mostly produces the over reduced product **4** (81.5 %) together with an 18.6 % of **6**, which comes from HDO processes. After 20 h reaction, **Ru@rGO/pyr-IMes$_{0.2}$** also shows complete conversion and a considerable amount of HDO products **5** (3.9 %) and **6** (16.7 %), but with a lower selectivity towards **4** (69.6 %). Comparing initial reaction rates of **Ru@rGO** and **Ru@rGO/pyr-IMes$_{0.2}$** (Figures 5a and 5b), the unmodified Ru NPs show the highest activity. After 1 hour of reaction, **Ru@rGO** exhibits an acetophenone conversion of 98 %, while the conversion by using **Ru@rGO/pyr-IMes$_{0.2}$** as catalyst is only 56 %. The initial reaction rate for **Ru@rGO/pyr-IMes$_{0.5}$** slightly decreases in comparison to **Ru@rGO/pyr-IMes$_{0.2}$** (Figures 5b and 5c), however, it was accompanied with an increase of the selectivity towards the fully hydrogenated product **4** and a significant drop in the formation of HDO products. More specifically, after 20 h, a conversion of *ca.* 98 % was achieved with a selectivity towards **4** of 84 %, producing only an 8.9 % of **6** (Table 1, entry 3). Upon increasing the number of equivalents of pyr-IMes up to 0.8 (**Ru@rGO/pyr-IMes$_{0.8}$**), we find a marked decrease in the activity, together with a substantial increase in the selectivity towards **2,** giving after 20h reaction 63.6 % of 1-phenylethanol at 96 % conversion (Figure 5d; Table 1, entry 4). Finally, the graphene-supported Ru NPs with the highest surface coverage, **Ru@rGO/pyr-IMes$_{1}$**, displays the lower activity, but the higher selectivity towards **2** (98 % selectivity at 60.2 % conversion), practically avoiding the formation of HDO products (Figure 5e; Table1, entry 5). These results show a clear correlation between the surface coverage degree and the activity and selectivity of the functionalized catalysts. The higher the amount of surface pyr-IMes ligands, the lower the activity of the catalyst, but the higher the selectivity towards **2**. In addition, at higher surface coverages the formation of HDO products is avoided. Both, the decrease in the activity and the selectivity improvement can be explained by a blocking of the ruthenium active sites by pyr-IMes ligands. As we increase the number of equivalents of pyr-IMes the amount of free ruthenium sites decreases, and, therefore, the activity is negatively affected. However, this blockage of active sites also improves the selectivity of the functionalized catalysts, not only avoiding the undesired HDO side reactions (*i.e.* **Ru@rGO/pyr-IMes$_{0.5}$**; Table 1, entry 3), but also hydrogenating selectively acetophenone to 1-phenylethanol at high surface coverages (*i.e.* **Ru@rGO/pyr-IMes$_{1}$**; Table 1, entry 5). It is important to mention that the selective hydrogenation of aromatic ketones to form benzyl alcohols is normally catalyzed by homogeneous catalysts,[40] since heterogeneous catalysts generally produces

View Article Online
DOI: 10.1039/D1CY02063C

**Table 2.** Hydrogenation reactions catalyzed by **Ru@rGO/pyr-IMes$_{0.5}$**.[a]

| Entry | Substrates | Products | Time (h) | Conversion (%)[b] | Selectivity (%)[b] |
|---|---|---|---|---|---|
| 1 | 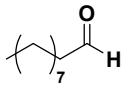 (7) | 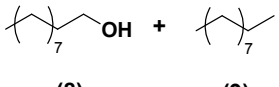 (8) (9) | 5 | >99 | **8:9** = 100:0 |
| 2 | 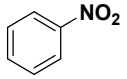 (10) | 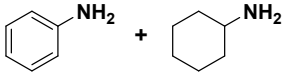 (11) (12) | 2 | >99 | **11:12** = 0:100 |
| 3 | 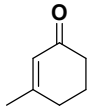 (13) | 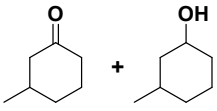 (14) (15) | 5 | >99 | **14:15** = 4:96 |
| 4 | 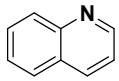 (16) | 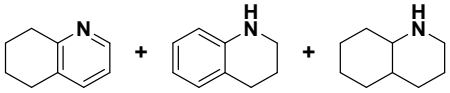 (17) (18) (19) | 5 | >99 | **17:18:19** = 0:9:91 |
| 5 | 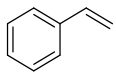 (20) | 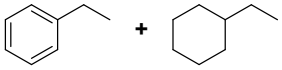 (21) (22) | 5 | >99 | **21:22** = 57:43 |
| 6 | 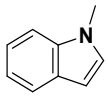 (23) | 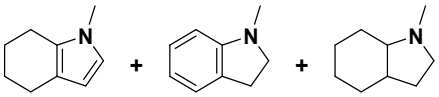 (24) (25) (26) | 5 | 96 | **24:25:26** = 9:1:90 |
| 7 | | | 20 | >99 | **24:25:26** = 0:0:100 |
| 8 | 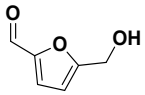 (27) | 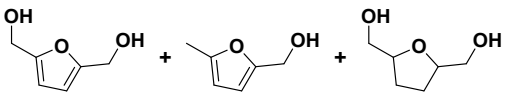 (28) (29) (30) | 5 | >99 | **28:29:30** = 92:2:6 |

[a] Reaction conditions: 0.5 mmol substrates, 0.5 mol% cat. (0.0025 mmol Ru), 10 mL THF, 50 bar $H_2$, 130 °C.

[b] Conversions and selectivities were determined by GC using dodecane as internal standard, and confirmed by GC-MS.

mixtures of **2**, **3** and **4**.[41] Altogether, these findings demonstrate that it is possible to control the selectivity of graphene-supported Ru NPs during acetophenone hydrogenation by modifying their metal surface with pyrene-tagged N-heterocyclic carbene ligands.

Among all the catalytic systems studied in the acetophenone hydrogenation reaction, **Ru@rGO/pyr-IMes$_{0.5}$**, is the most attractive one since it presents the best compromise between activity and selectivity. This functionalized catalyst hydrogenates selectively acetophenone to 1-cyclohexylethanol, minimizing the generation of HDO products (Figure 5f; Table 1, entry 3). Therefore, **Ru@rGO/pyr-IMes$_{0.5}$** was also tested in the hydrogenation of various substrates that contain other reducible functional groups such as aldehyde, vinyl, heterocyclic or nitro groups, under the same catalytic conditions (Table 2). Decanal (**7**) was selectively hydrogenated to 1-decanol (**8**) after 5 h reaction, without formation of the HDO product **9** (Table 2, entry 1). After 2h, nitrobenzene (**10**) was also selectively converted to cyclohexylamine (**12**) (Table 2, entry 2). Similar reactivity was observed in the hydrogenation of 3-methyl-2-cyclohexenone (**13**) and quinoline (**16**). Both substrates, after 5 h, gave full conversion with high selectivity towards the corresponding over reduced product (Table 2, entries 3 and 4). On the other hand, at the same reaction time, styrene (**20**) only produced 43 % of ethylcyclohexane (**22**). Furthermore, we investigated the catalytic activity of **Ru@rGO/pyr-IMes$_{0.5}$** in other molecules of current interest such as 1-methylindole (**23**), which can be used as liquid hydrogen carrier (LOHCs), or 5-(hydroxymethyl)furfural (HMF; **27**), a platform molecule derived from biomass. After 5 h reaction, **Ru@rGO/pyr-IMes$_{0.5}$** presented a 96 % conversion of **23** with 90 % selectivity towards the completely hydrogenated product 1-methyl-octahydroindole (**22**) (Table 2, entry 6). At longer reaction times (20h), a complete conversion with 100% selectivity to **22** was achieved (Table 2, entry 7).These results are of high interest for hydrogen storage applications, since 1-methylindole is a promising LOHC due to its low melting point (-20 °C) and high hydrogen content (5.76 wt%).[42] Due to the

View Article Online
DOI: 10.1039/D1CY02063C



**Table 3.** Mean diameter of graphene-supported Ru NPs before and after catalysis.

| Entry | Catalyst | Size before catalysis (nm) | Size after catalysis (nm) |
|---|---|---|---|
| 1 | **Ru@rGO** | 1.5 ± 0.5 | 2.3 ± 0.5 |
| 2 | **Ru@rGO/pyr-IMes$_{0.2}$** | 1.5 ± 0.4 | 2.1 ± 0.5 |
| 3 | **Ru@rGO/pyr-IMes$_{0.5}$** | 1.5 ± 0.3 | 1.9 ± 0.3 |
| 4 | **Ru@rGO/pyr-IMes$_{0.8}$** | 1.5 ± 0.7 | 1.8 ± 0.4 |
| 5 | **Ru@rGO/pyr-IMes$_1$** | 1.5 ± 0.4 | 1.7 ± 0.4 |
| 6 | **Ru@rGO/ICy$_1$** | 1.6 ± 0.5 | 2.3 ± 0.5 |

great potential of this functionalized catalyst, **Ru@rGO/pyr-IMes$_{0.5}$** have been also tested in the hydrogenation of an interesting biomass derived platform molecule, *i.e.* HMF (**27**). After 5 h of reaction, **Ru@rGO/pyr-IMes$_{0.5}$** showed a quantitative conversion with excellent selectivity towards 5-bis(hydroxymethyl)furan (BHMF) (**28**) (92 %; Table 2, entry 8). HDO and hydrogenation products **29** and **30** were also formed, but in minute amounts.

A series of experiments were performed to investigate the influence of the surface pyrene-tagged NHCs on the stability of graphene-supported Ru NPs. First, we analyzed by TEM the size and morphology of Ru NPs present on the unmodified and modified catalytic systems after a standard catalytic test (hydrogenation of acetophenone during 20h at 130 bar $H_2$ and 130 $^oC$). The Ru NPs supported on **Ru@rGO** significantly increased their size from 1.5 to 2.3 nm (Table 3, entry 1). On the other hand, Ru NPs on **Ru@rGO/pyr-IMes$_1$** practically did not increase in size after catalysis (from 1.6 to 1.7 nm; Table 3, entry 5). The analysis after catalysis of the Ru NPs immobilized on the other three functionalized catalytic systems showed intermediate sizes. More specifically, we observed that the main diameter of the nanoparticles after catalysis decreases as the number of equivalents of pyr-IMes in the system increases (Table 3, entries 2-4). Therefore, there is an evident correlation between the amount of surface NHC ligands and the stability of the supported Ru NPs against sintering (Figures S16-S20). The higher the surface coverage, the more resistant to sintering is the catalyst. This demonstrates the ability of the pyr-IMes ligands to increase the stability of graphene-supported MNPs, as previously reported for similar systems.[3b]

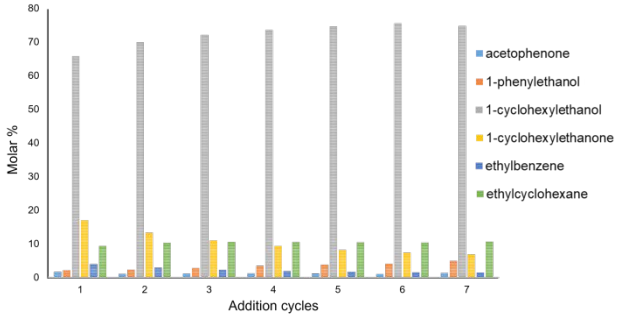


**Figure 6.** Multiple addition experiment for the hydrogenation of acetophenone catalyzed by **Ru@rGO/pyr-IMes$_{0.5}$**. Conditions: acetophenone (0.5 mmol), 0.5 mol % cat. (0.0025 mmol metal), THF, 50 bar $H_2$, 130 °C, 12 h. Every 12 hours, acetophenone (0.5 mmol) was added to the reaction mixture. Conversions and selectivities were determined by GC using dodecane as the internal standard, and confirmed by GC-MS

The influence of the pyrene tag on the activity/selectivity and stability of **Ru@rGO/pyr-IMes** was evaluated by using as modifier another NHC ligand without polyaromatic groups on the N-substituents. Concretely, **Ru@rGO** was functionalized with 1 equiv. of an NHC with cyclohexyl groups on the N-substituents (1,3-dicyclohexylimidazol-2-ylidene; ICy) following the two-step synthetic route of Figure 1 (**Ru@rGO/ICy$_1$**) (Figure S21). In this case, the absence of the pyrene tag affected both the selectivity and stability of the resulting catalyst. After studying the reactivity of **Ru@rGO/ICy$_1$** during the hydrogenation of acetophenone, we observed that it was not possible to control the selectivity of the catalyst in the same way as with **Ru@rGO/pyr-IMes$_1$** (Figure S22). Here, even at high NHC surface coverage (1 equiv. of ICy), we observed the hydrogenation of both functional groups (carbonyl and phenyl), being the totally hydrogenated product **4** the main product after 20 h (Table 1, entry 6). Probably, the lack of aromatic groups of ICy allows the interaction between the acetophenone and the faces of the Ru NPs, and thus the hydrogenation of phenyl groups. Already reported surface studies on colloidal Ru nanoparticles stabilized by ICy confirm the presence of free available faces.[23b] Contrary to the pyr-IMes ligands, which through π-interactions block the ruthenium terraces of **Ru@rGO/pyr-IMes$_1$**, hydrogenating selective acetophenone (**1**) to 1-phenylethanol (**2**). The surface modification of **Ru@rGO** with ICy neither controls the formation of HDO side-products **5** and **6**. By analyzing the size of Ru NPs present on **Ru@rGO/ICy$_1$** before and after the standard catalytic test (hydrogenation of acetophenone) by TEM (Table 3, entry 6; Figures S23 and S24), we observed a noticeable increase in size ,from 1.5 to 2.3 nm, similar to that observed in the unmodified **Ru@rGO**. In addition, the nanoparticle distribution observed after catalysis is much less uniform (Figure S24). The absence of π-interactions between the ICy ligands and the graphene layer, explains the lower stability of these Ru NPs against sintering. Altogether, these results highlight the importance of the presence of the pyrene tag in the NHC used as modifier to control the selectivity and the stability of these functionalized catalysts.

To test the recyclability of **Ru@rGO/pyr-IMes$_{0.5}$** a multiple addition experiment was performed. Specifically, the hydrogenation of acetophenone was carried out during seven consecutive additions of substrate (each 12 h) using **Ru@rGO/pyr-IMes$_{0.5}$** as catalyst. Interestingly, we observed that the catalyst not only kept the activity during this multi-addition experiment, but also improved the selectivity to 1-cyclohexyletanol (**4**) (Figure 6). This progressive increase in the reactivity during the first addition cycles is explained by the formation of a more active surface under catalytic conditions, due to the gradual reduction of the Ru metal surface (which is partially oxidized in the as-synthesized Ru NPs as was observed by XPS). TEM analysis of **Ru@rGO-pyr-IMes$_{0.5}$** after the multi-addition experiment revealed Ru NPs similar in size and distribution to the as-prepared ones (Figure S25). These results underline the high stability of this functionalized catalyst under catalytic conditions during long reaction times (up to 86 h).

View Article Online
DOI: 10.1039/D1CY02057C





Finally, to verify the heterogeneous nature of **Ru@rGO-pyr-IMes$_{0.5}$**, a "hot filtration" experiment was performed during the hydrogenation reaction of acetophenone (130 °C, 50 bar $H_2$). After 2h reaction, the solid **Ru@rGO-pyr-IMes$_{0.5}$** was separated by thermal filtration and the mother liquor solution was transferred to an empty reactor and then pressurized and heated. No change in the conversion was observed after 4 hours under the same catalytic conditions. Specifically, the conversion was maintained at 59 % (Table S3, see ESI), while 88 % conversion was observed in the presence of **Ru@rGO/pyr-IMes$_{0.5}$** (Figure 5c). In addition, ICP analysis after the thermal filtration did not show any metal leaching (see the Experimental Section), confirming the heterogeneity of the catalyst.

## Conclusions

Catalytic properties of graphene-supported Ru NPs were finely tuned by modifying their metal surface with pyrene-tagged NHC ligands. A combined study comprising EA and BET surface area analysis allowed us to determine the precise amount of pyr-IMes incorporated into the different functionalized catalysts. CO chemisorption studies confirmed both the coordination of NHC ligands to the ruthenium surface and the presence of free Ru sites on these functionalized catalysts. Ligand-stabilized Ru NPs were used as model catalysts for surface studies. The results suggested the presence of a second coordination sphere of pyr-IMes ligands on these non-supported Ru NPs, probably formed by π–π stacking interactions between the aromatic groups of the pyrene-tagged NHCs. Despite the high surface coverage of these non-supported Ru NPs, they still have a large number of available active sites, as it was confirmed by DRIFT and solid-state NMR analyses using CO as molecular probe. Interestingly, by XPS we were able to distinguish the different nature and interaction modes of pyr-IMes ligands on the functionalized catalysts. For example, in **Ru@rGO/pyr-IMes$_{0.5}$**, the pyrene-tagged NHC can be found in three different ways: (i) as a protonated carbene, (ii) coordinated to the ruthenium surface and (iii) directly interacting with the graphene support. According to the catalytic results, we observed that both the activity and selectivity of these graphene-supported Ru NPs were highly dependent on the surface coverage degree. This clear correlation was investigated using acetophenone hydrogenation as a model reaction. The higher the amount of surface NHC ligands, the lower the activity of the catalyst, but the higher the selectivity towards 1-phenylethanol. Moreover, at higher surface coverages the hydrodeoxygenation side-reaction is practically suppressed. This increase in the selectivity at the expense of the activity is explained by a blockage of metal active sites by surface ligands. The reactivity of **Ru@rGO/pyr-IMes$_{0.5}$**, which displays the best balance between activity and selectivity, was also evaluated in the hydrogenation of other substrates of interest, such as 1-methylindole or HMF, among others. Finally, the stability of the modified and non-modified catalysts was studied by TEM analysis after catalysis, observing an evident correlation between the nanoparticle surface ligand coverage and the stability of the supported Ru NPs against sintering. The presence of the pyrene tag on the NHC used as modifier is crucial to control both the selectivity and stability of these ligand-functionalized supported Ru NPs. In addition, **Ru@rGO/pyr-IMes$_{0.5}$** was employed in multi-addition and "hot filtration" experiments, showing a high stability and recyclability. To sum up, these results prove that it is possible to control the activity, selectivity and stability of graphene-supported Ru NPs by modifying their metal surface with organic molecules, making them potential catalysts for industrial applications, since they unify the benefits of homogeneous (high selectivity) and heterogeneous (stability and recyclability) catalysts.

## Experimental

**General methods.**

Most chemical operations performed in this work were carried out using conventional Fischer-Porter techniques, Schlenk tubes and glovebox under nitrogen atmosphere. Solvents were purified before use, THF (Sigma-Aldrich) by distillation under argon atmosphere through filtration in the column of a solvent purification system (SPS). The organometallic ruthenium precursor, (1,5-cyclooctadiene)(1,3,5-cyclooctatriene) Ruthenium(0), [Ru(COD)(COT)], was purchased from Nanomeps (Toulouse), rGO from Graphenea and acetophenone (99 %), decanal (98 %), nitrobenzene (99 %), styrene (99 %), 3-methyl-2-cyclohexenone (98 %), quinoline (98 %), 1-methylindole (> 97 %), dodecane (99 %) and 1,3-dicyclohexylimidazolium chloride from Merck. All reagents were used without prior purification, except for HMF (97 %, Carbosynth) which is purified by filtering with an equimolar silica:alumina mixture, and stored in a refrigerator.

*Transmission Electron Microscopy (TEM) and High-Resolution Transmission Electron Microscopy (HRTEM).* Non-supported and supported Ru NPs, were analyzed by TEM and HRTEM. For sample preparation, a small amount of the isolated materials was adequately dispersed in THF and an aliquot was deposited on a copper grid. TEM and HRTEM analyses were performed at the "Servicio de Microscopia Electrónica" of Universitat Politècnica de València (UPV). HRTEM analysis were carried out with a JEOL JEM 2010 electron microscope with a working voltage of 200 kV with a resolution point of 2.35 Å. FFT (Fast Fourier Transform) treatments have been carried out with the DigitalMicrograph program version 3.7.4. TEM observation were performed by using a JEOL JEM 1400Flash electron microscope operating at 120 kV with a point resolution of 3.8 Å. The measurement of the size distribution of the nanoparticles was performed with ImageJ program by analyzing their length on a given area of the copper grid.

*Elemental Analysis (EA).* Measurements were carried out in a Euro EA3000 Elemental Analyzer (EuroVector), using sulfanilamide as a reference standard.

*Gas Chromatography (GC).* The spectra of the reactants and their hydrogenated products were recorded with an Agilent

Technologies 7890A GC-system with Flame ionization detector and a HP-5 column. The method used starts with the injection temperature T0. After holding this temperature for 2 min, the column is heated to temperature T1 (10 °C/min) and finally, the column is heated to T2 (30 °C/min) and hold for 1 min (T0 = 80 °C, T1 = 160 °C, T2 = 280 °C). On the other hand, HMF and derivatives spectra were obtained with Varian CP-3800 equipment with a Varian CP-8400 automatic injector and a Carbowax column. The method used starts with an injection temperature of 50 °C. After hold the temperature for 1 minute, the column is heated to a 240 °C (20 °C/min) maintaining this temperature 3.5 minutes. Dodecane has been used as an internal standard.

*Gas Cromatography-Mass Spectrometry (GC-MS).* GC-MS analyses were carried out in an Agilent 6890N chromatograph equipped with a HP-5 column (30 m, 0.32 mm, 0.25 µm), coupled to Agilent 5973N electron impact mass spectrometer.

*Inductively Coupled Plasma Optical Emission Spectrometry (ICP-OES).* Digestion of the graphene supported Ru NPs were performed in a microwave oven for an hour by adding a 3:1 solution of nitric and hydrochloric acid for 12h. The ICP analysis were performed with Agilent 7500 CX. Metal content of ligand stabilized Ru NPs (**Ru/pyr-IMes$_{0.2}$** and **Ru/pyr-IMes$_{0.5}$**) were measured by Kolbe MikroLab by ICP-AES.

Raman spectroscopy. For the measurement of the Raman spectra, excitation wavelengths of 514 and/or 785 nm were set in a "*Renishaw In* via" Raman spectrometer equipped with a Lyca microscope. The samples (powder) were deposited in an aluminum support and measured within the region of 0 to 3000 $cm^{-1}$ with a resolution of <4$cm^{-1}$.

X-Ray Photoelectron Spectroscopy (XPS). XPS analyses were performed using a SPECS device equipped with a Phoibos 150-9MCD detector using Mg-Kα radiation (hυ=1235.6 eV) and Al-Kα radiation (hυ=1483.6 eV) from a dual source. During the measurements, pressure was maintained below $10^{-9}$ Torr. The quantification and evaluation of the spectra has been carried out with the help of the *CASA* software, referencing based on C1s = 284.5 eV.

Solid-state Magic Angle Spinning Nuclear Magnetic Resonance (MAS-NMR) spectroscopy. MAS-NMR analyses with and without $^{1}H$-$^{13}C$ cross-polarization (CP) were performed at the ITQ on a Bruker Avance 400WB instrument equipped with a 3.2 mm probe and with a sample rotation frequency of 10 kHz. Measurements were made in a 3.2 mm $ZrO_2$ rotor.

Chemisorption. CO adsorption measures were taken using the double isotherm method on a Quantachrome Autosorb-1C equipment. Prior to adsorption, the samples were reduced in situ in flowing pure hydrogen (25 mL/min) at 200ºC for 3 h (10 ºC/min rate). After reduction, the samples were degassed at 1333x$10^{-3}$ Pa for 2 h at the reduction temperature, and then the temperature was lowered at 25 ºC (1 hour for cooling down the sample to adsorption temperature). Then, pure CO was admitted and the first adsorption isotherm (i.e. the total CO uptake) was measured. After evacuation at 25 ºC, the second isotherm (i.e. the reversible CO uptake) was taken. The amount of chemisorbed CO was then obtained by subtracting the two isotherms. The pressure range studied was 0.5 - 11 x $10^4$ Pa.

BET. The isotherms were recorded with a Micrometrics ASAP-2000 at the temperature of -196ºC. The samples were vacuum treated for 24 hours before adsorption measurements that were carried out at a temperature of 120 ºC.

Diffuse Reflectance Infrared Fourier Transform spectroscopy (DRIFT). DRIFT measurements were taken on a Bruker Vertex 70 equipment with a 3 mm aperture, 20 KHz speed and a resolution of 4 $cm^{-1}$. The samples were prepared by dropping a drop of a THF solution of the ligand (pyr-IMes) or the colloidal nanoparticles (**Ru@pyr-IMes**), before and after bubbling CO during 5 min, on a well with KBr, which was placed in the cell.

**Synthesis of pyr-IMes·HBr**

The synthesis of the imidazolium salt (pyr-IMes·HBr) was obtained following a synthetic method previously described elsewhere.[32]

**Synthesis of graphene-supported Ru NPs.**

**Ru@rGO.** A Schlenk flask was charged with 10 mg (0.032 mmol) of Ru(COD)(COT) and dissolved in 3 mL of anhydrous and deoxygenated THF. After that, the solution was added to a 250 mL Fischer-Porter bottle with a 100 mg suspension of reduced graphene oxide (rGO) in 50 mL of THF previously sonicated during 90 min. The Fischer-Porter was then pressurized with 3 bar $H_2$ and the dispersion was stirred vigorously during 20 h at room temperature. After that, the pressure was released and **Ru@rGO** was filtered through a polyamide membrane (Whatman® membrane filters, 47mmx0.45µm) under vacuum and washed with 100 mL of THF. Finally, the catalyst was dried in an oven overnight at 60 ºC. The mean particle size value obtained for **Ru@rGO** was 1.5 ± 0.5 nm. ICP measurements showed that the catalyst contained 2.45 wt% of metal.

**Ru@rGO/pyr-IMes$_{0.2}$.** A Schlenk flask was charged with 10 mg (0.032 mmol) of Ru(COD)(COT) and dissolved in 3 mL of anhydrous and deoxygenated THF. After that, the solution was added to a 250 mL Fischer-Porter bottle with a 100 mg suspension of reduced graphene oxide (rGO) in 50 mL of THF previously sonicated during 90 min. The Fischer-Porter was then pressurized with 3 bar $H_2$ and the dispersion was stirred vigorously during 20 h at room temperature. At the same time, a Schlenk flask was charged with pyr-IMes·HBr (3.1 mg, 0.0063 mmol, 0.2 equiv.) and potassium tert-butoxide (0.9 mg, 0.0079 mmol, 0.25 equiv.) and dissolved in 5 mL of deoxygenated and dehydrated THF from the SPS. After 20 h stirring at room temperature, the resulting suspension was filtered through dry Celite (1 cm) under argon atmosphere and transferred to the Fischer-Porter bottle charged with **Ru@rGO** (where hydrogen pressure was released previously). The stirring was kept for 1 h, and the resulting solid was filtered through a polyamide membrane (Whatman® membrane filters, 47mmx0.45µm) under vacuum and washed with 100 mL of THF. Finally, the black precipitate was dried overnight in an oven at 60 ºC. The nanoparticle size was measured by TEM on a population of at least 100 NPs, which afforded a mean value of 1.5 ± 0.4 nm. ICP measurements showed that the catalyst contained 2.43 wt% of metal.

**Ru@rGO/pyr-IMes$_{0.5}$.** For this synthesis, the procedure described for **Ru@rGO/pyr-IMes$_{0.2}$** has been followed, but adding instead 7.6 mg (0.0159 mmol, 0.5 equiv.) of pyr-IMes·HBr and 2 mg (0.0174 mmol, 0.55 equiv.) of K$^t$BuO. The mean particle size value obtained was 1.5 ± 0.3 nm. ICP measurements showed that the catalyst contained 2.48 wt% of metal.

**Ru@rGO/pyr-IMes$_{0.8}$.** For this synthesis, the procedure described for **Ru@rGO/pyr-IMes$_{0.2}$** has been followed, but adding instead 12.2 mg (0.0253 mmol, 0.8 equiv.) of pyr-IMes·HBr and 3 mg (0.0270 mmol, 0.88 equiv.) of K$^t$BuO. The mean particle size value was 1.6 ± 0.7 nm. ICP measurements showed that the catalyst contained 2.50 wt% of metal.

**Ru@rGO/pyr-IMes$_1$.** For this synthesis, the procedure described in **Ru@rGO/pyr-IMes$_{0.2}$** has been followed, but adding instead 15.3 mg (0.0317 mmol, 1 equiv.) of pyr-IMes·HBr and 3.7 mg (0.0333 mmol, 1.1 equiv.) of K$^t$BuO. The mean particle size value obtained was 1.6 ± 0.4 nm. ICP measurements showed that the catalyst contained 2.32 wt% of metal.

**Ru@rGO/ICy$_1$.** For this synthesis, the procedure described in **Ru@rGO/pyr-IMes$_{0.2}$** has been followed, but adding instead 8.5 mg (0.0317 mmol, 1 equiv.) of ICy·HCl and 3.7 mg (0.0333 mmol, 1.1 equiv.) of K$^t$BuO. The mean particle size value obtained was 1.6 ± 0.5 nm

**Synthesis of ligand-stabilized Ru NPs.**

**Ru/pyr-IMes$_{0.2}$.** A Schlenk flask was charged with pyr-IMes·HBr (30.5 mg, 0.0634 mmol, 0.2 equiv.) and K$^t$BuO (10 mg, 0.0793 mmol, 0.25 equiv.) and dissolved in 10 mL of deoxygenated and dehydrated THF from the SPS. After that the solution was added to a 250 mL Fischer-Porter bottle charged with a cooled solution (-80 °C) of Ru(COD)(COT) (100 mg, 0.32 mmol) in 50 mL of THF (previously degassed by three freeze-pump cycles). The Fischer-Porter was then pressurized with 3 bar of $H_2$, and the solution was allowed to reach room temperature while the solution was stirred vigorously. A black homogeneous solution was immediately formed, and the stirring was kept for 20 hours at room temperature. After that, the remaining $H_2$ pressure was released with vacuum, and 50 mL of anhydrous pentane was added to the solution to favour the precipitation of **Ru/pyr-IMes$_{0.2}$** NPs, and then they were dried overnight under vacuum. The size of the NPs was measured by TEM image on a sample of a least 100 nanoparticles, which afforded a mean value of 1.4 ± 0.4 nm. ICP gave the following Ru content: 55.7 %.

**Ru/pyrIMes$_{0.5}$.** Same procedure as previously described for **Ru/pyr-IMes$_{0.2}$** has been followed, with the difference that 76.3 mg (0.1585 mmol, 0.5 equiv.) of pyr-IMes·HBr and 25 mg (0.1744 mmol, 0.55 equiv.) of K$^t$BuO were added**.** The size of the nanoparticles was measured by TEM analyzing a sample which contained at least 100 particles, obtaining an average value of 1.3 ± 0.4 nm. The metallic content has been quantified by ICP, giving an experimental Ru content of 33.2%.

**Synthesis of pyr-IMes/rGO**

**pyr-IMes/rGO.** A Schlenk flask was charged with 7.6 mg (0.0159 mmol, 0.5 equiv.) of pyr-IMes·HBr and 2 mg (0.0174 mmol, 0.55 equiv.) of K$^t$BuOH and dissolved in 5 mL of deoxygenated and dehydrated THF. The solution was stirred vigorously for 20 h at room temperature. After that, a Fischer-Porter bottle was charged with 100 mg of reduced graphene oxide (rGO) and dissolved in 50 mL of anhydrous and deoxygenated THF. The solution was sonicated 90 min for ensure its dispersion. Later, pyr-IMes$_{(0.5)}$ solution was filtered through dry Celite (1 cm) under argon atmosphere and transferred to the Fischer-Porter bottle charged with rGO. The stirring was kept for 1 h, and the resulting solid is filtered through a polyamide membrane (Whatman® membrane filters, 47mmx0.45µm) under vacuum and washed with 100 mL of THF. Finally, the black precipitate was dried overnight in an oven at 60 °C.

**Catalytic hydrogenation reactions.**

The hydrogenation of acetophenone, 1-methylindole, quinoline and HMF were performed in a 25 mL autoclave engineer reactor, equipped with a mechanical stirrer (750 rpm). Hydrogenations were carried out so that the metal-substrate molar ratio was 1:200. In this way, considering that 0.5 mmol of substrate was used and each catalyst has 3 wt% of the Ru metal, 0.5 mol% of metal-catalyst was added in each reaction, which means 0.0025 mmol of metal in each case. For all the immobilized and functionalized catalysts, the exact mass added during the catalysis were 10 mg.

Thus, 10 mg of the catalyst was dispersed in 9 mL of THF sonicating for 60 minutes. The suspension was transferred into the reactor, which was purged with $H_2$ three times, and finally pressurized with 35 bar of $H_2$. The reactor was then heated at 150 °C, reaching a final pressure of 50 bar. The catalyst is kept under these conditions for one hour, to reduce and activate the active ruthenium species. Before the substrate (0.5 mmol) and dodecane (0.3 mmol) diluted in 1 mL of THF were injected with the help of a 250 µL Hamilton syringe, the temperature is reduced to 130 °C. After maintained the reaction for 20 h, the reactor temperature is lowered to room temperature and depressurized. The resulting suspension is collected, and a fraction is filtered to separate the catalyst from the rest of the solution, which is analyzed by GC and GC-MS.

**Kinetic experiments.**

For the kinetic experiments, the reactor was charged, pressurized and heated at the required conditions and aliquots were taken from the reaction medium every hour. Then, the aliquot was analyzed by GC using dodecane as internal standard.

**Multiple addition experiments.**

For the multiple addition experiment, the autoclave was charged, pressurized and heated at the required conditions for acetophenone hydrogenation (130 °C, 50 bar $H_2$, 10 mL THF). Every 12 hours, an aliquot was taken from the reaction medium and new starting substrate (i.e. acetophenone) was added to the reactor. The aliquots were analyzed by GC using dodecane as internal standard, and confirmed by GC-MS. The activity and

selectivity remained over 7 catalytic cycles confirming the stability of the Ru-NP catalysts.

**"Hot filtration" experiment**

For the "hot filtration" experiment, the reactor was charged, pressurized and heated under the required conditions for acetophenone hydrogenation (130 °C, 50 bar $H_2$, 10 ml THF). After 2 h reaction, **Ru@rGO/pyr-IMes$_{0.5}$** was removed by thermal filtration, and another clean and empty autoclave was charged with the mother liquor solution, pressurized and heated under the same reaction conditions. Then, the conversion of acetophenone was determined after 4 h and compared to that at 2 h (Table S2, ESI). No change in the conversion was observed. After the "hot filtration", the mother liquor solution was analyzed by ICP, being the Ru detected negligible.

## Author Contributions

C.C-N. and A.G-Z. performed the synthesis and structural/spectroscopic characterization and catalytic experiments and participated in writing - review and editing. A.M-C. performed the synthesis and spectroscopic characterization of the NHC ligands. P.O-B., A.C and J.M. supervised the project and participated in writing - review and editing. LM.M-P. conceived the idea of the project and wrote the original draft with input from other authors. All authors contributed to the design of experiments, analysis of the results and preparation of the manuscript.

## Conflicts of interest

There are no conflicts to declare.

## Acknowledgements

The authors thank Instituto de Tecnología Química (ITQ), Consejo Superior de Investigaciones Científicas (CSIC), Universitat Politècnica de València (UPV) and 'Servei Central d'Instrumentació Científica (SCIC) de la Universitat Jaume I' for the facilities and MICIU/AEI/FEDER (RTI2018-098237-B-C22 and Universitat Jaume I (UJI-B2018-23) for the financial support. We also thank the Electron Microscopy Service of the UPV for TEM facilities, Jose A. Vidal-Moya (ITQ, CSIC-UPV) for MAS-NMR measurements and J. Gaona for his assistance in catalytic reactions. A. G.-Z. acknowledges to "*Programa de Ayudas del Aula Cemex Sostenibilidad*" for the completion of the Master's Thesis in Sustainable Chemistry and C. C.-N. gratefully thanks Generalitat Valenciana predoctoral fellowship (GVA: ACIF/2019/076). A. M-C. thanks Generalitat Valenciana for grant (ACIF/2019/100).

## Notes and references

1 a) D. Astruc, *Chem. Rev.*, 2020, **120**, 461. b) P. Serp and K. Philippot, *Nanomaterials in Catalysis*; Wiley-VCH: Weinheim, Germany, 2013. c) D. Astruc, *Nanoparticles and Catalysis*, Wiley-VCH: Weinheim, Germany, 2008.

2 D. Astruc, F. Lu and J. R. Aranzaes, *Angew. Chem. Int. Ed.*, 2005, **44**, 7852.

3 a) M. R. Axet and K. Philippot, *Nanoparticles in Catalysis: Advances in Synthesis and Applications*, Wiley-VCH: Weinheim, Germany, 2021; b) L. M. Martínez-Prieto and P. W. N. M. van Leeuwen, *Ligand effects in ruthenium nanoparticle catalysis*, 2020, pp.407-448.

4 M. R. Axet and K. Philippot, *Chem. Rev.*, 2020, **120**, 1085.

5 a) C. A. Schoenbaum, D. K. Schwartz and J. W. Medlin, *Acc. Chem. Res.*, 2014, **47**, 1438. b) S. Kunz, *Top. Catal.,* 2016, **59**, 1671.

6 a) K. R. Kahsar, D. K. Schwartz and J. W. Medlin, *J. Am. Chem. Soc.,* 2014, **136**, 520. b) I. Schrader, S. Neumann, A. Šulce, F. Schmidt, V. Azov and S. Kunz, *ACS Catal.,* 2017, **7**, 3979. c) P. D. Coan, L. D. Ellis, M. B. Griffin, D. K. Schwartz and J. W. Medlin, *J. Phys. Chem. C* 2018, **122**, 6637. d) A. Šulce, J. Backenköhler, I. Schrader, M. D. Piane, C. Müller, A. Wark, L. C. Ciacchi, V. Azov and S. Kunz, *Catal. Sci. Tech.,* 2018, **8**, 6062. e) P. D. Coan, C. A. Farberow, M. B. Griffin and J. W. Medlin, *ACS Catal.,* 2021, **11**, 3730.

7 a) M. J. Climent, A. Corma and S. Iborra, *Chem. Rev.*, 2011, **111**, 1072. b) A. Corma and H. Garcia, *Top. Catal.*, 2008, **48**, 8.

8 Q. L. Zhu and Q. Xu, *Chem*, 2016, **1**, 220.

9 a) Y.-Z. Chen, G. Cai, Y. Wang, Q. Xu, S.-H. Yu and H.-L. Jiang, *Green Chem.*, 2016, **18**, 1212. b) A. Noujima, T. Mitsudome, T. Mizugaki, K. Jitsukawa and K. Kaneda, *Angew. Chem. Int. Ed.*, 2011, **50**, 2986.

10 S. Navalon, A. Dhakshinamoorthy, M. Alvaro and H. Garcia, *Coord. Chem. Rev.*, 2016, **312**, 99.

11 J. Lee, K. S. Novoselov and H. S. Shin, *ACS Nano* 2011, **5**, 608.

12 a) E. D. Grayfer, L. S. Kibis, A. I. Stadnichenko, O. Y. Vilkov, A. I. Boronin, E. M. Slavinskaya, O. A. Stonkus and V. E. Fedorov, *Carbon* 2015, **89**, 290. b) D. E. García-Rodríguez, L. H. Mendoza-Huizar and C. Díaz, *Appl. Surf. Sci.*, 2017, **412**, 146. c) I. Fampiou and A. Ramasubramaniam, *J. Phys. Chem. C* 2012, **116**, 6543.

13 A. J. Arduengo III, R. L. Harlow and M. Kline, *J. Am. Chem. Soc.*, 1991, **113**, 361.

14 a) W. A. Herrmann, J. GoobenL and M. Spiegler, *J. Organomet. Chem.,* 1997, **547**, 357. b) M. Poyatos, J. A. Mata and E. Peris, *Chem. Rev.,* 2009, **109**, 3677. c) L. A. Schaper, S.J. Hock, W.A. Herrmann and F.E. Kühn, *Angew. Chem. Int. Ed.*, 2012, **52**, 270.

15 M. N. Hopkinson, C. Richter, M. Schedler and F. Glorius, *Nature* 2014, **510**, 485.

16 a) M. Koy, P. Bellotti, M. Das and F. Glorius, *Nat. Catal.*, 2021, **4**, 352. b) C. A. Smith, M. R. Narouz, P. A. Lummis, I. Singh, A. Nazemi, C. H. Li and C. M. Crudden, *Chem. Rev.*, 2019, **119**, 4986. c) C. Cerezo-Navarrete, P. Lara and L. M. Martínez-Prieto, *Catalysts* 2020, **10**, 1144.

17 E. C. Hurst, K. Wilson, I. J. S. Fairlamb and V. Chechik, *New J. Chem.*, 2009, **33**, 1837.

18 U. Hintermair, S. M. Hashmi, M. Elimelech and R. H. Crabtree, *J. Am. Chem. Soc.*, 2012, **134**, 9785.

19 a) P. Lara, O. Rivada-Wheelaghan, S. Conejero, R. Poteau, K. Philippot and B. Chaudret, *Angew. Chem. Int. Ed.,* 2011, **50**, 12080. b) L. M. Martínez-Prieto, E. A. Baquero, G. Pieters, J. C. Flores, E. De Jesús, C. Nayral, F. Delpech, P. W. N. M. Van Leeuwen, G. Lippens and B. Chaudret, *Chem. Commun.*, 2017, **53**, 5850.

20 M. D. de los Bernardos, S. Perez-Rodriguez, A. Gual, C. Claver and C. Godard, *Chem. Commun.,* 2017, **53**, 7894.

21 K. V. S. Ranganath, J. Kloesges, A. H. Schäfer and F. Glorius, *Angew. Chem. Int. Ed.*, 2010, **49**, 7786.

22 a) E. A. Baquero, S. Tricard, J. C. Flores, E. de Jesús and B. Chaudret, *Angew. Chem.*, 2014, **126**, 13436. b) E. A. Baquero, S. Tricard, Y. Coppel, J. C. Flores, B. Chaudret and E. De Jesús, *Dalton Trans.*, 2018, **47**, 4093.

23 a) C. Richter, K. Schaepe, F. Glorius and B. J. Ravoo, *Chem. Commun.*, 2014, **50**, 3204. b) L. M. Martínez-Prieto, A. Ferry, P. Lara, C. Richter, K. Philippot, F. Glorius and B. Chaudret, *Chem. Eur. J.*, 2015, **21**, 17495. c) L. M. Martinez-Prieto, A. Ferry, L. Rakers, C. Richter, P. Lecante, K. Philippot, B. Chaudret and F. Glorius, *Chem. Commun.,* 2016, **52**, 4768.

24 a) L. M. Martínez-Prieto, L. Rakers, A. M. López-Vinasco, I. Cano, Y. Coppel, K. Philippot, F. Glorius, B. Chaudret and P. W. N. M. van Leeuwen, *Chem. Eur. J.,* 2017, **23**, 12779. b) L.C. Moraes, R.C. Figueiredo, J.P. Espinós, F. Vattier, A. Franconetti, C. Jaime, B. Lacroix, J. Rojo, P. Lara and S. Conejero. *Nanoscale* **2020**, 12, 6821.

25 a) C. Taglang, L. M. Martínez-Prieto, I. del Rosal, L. Maron, R. Poteau, K. Philippot, B. Chaudret, S. Perato, A. Sam Lone, C. Puente, C. Dugave, B. Rousseau and G. Pieters, *Angew. Chem.*, 2015, **127**, 10620. b) A. Palazzolo, S. Feuillastre, V. Pfeifer, S. Garcia-Argote, D. Bouzouita, S. Tricard, C. Chollet, E. Marcon, D.-A. Buisson, S. Cholet, F. Fenaille, G. Lippens, B. Chaudret and G. Pieters, *Angew. Chem. Int. Ed.,* 2019, **58**, 4891.

26 a) D. Gonzalez-Galvez, P. Lara, O. Rivada-Wheelaghan, S. Conejero, B. Chaudret, K. Philippot and P. W. N. M. Van Leeuwen, *Catal. Sci. Technol.*, 2013, **3**, 99. b) P. Lara, A. Suárez, V. Collière, K. Philippot and B. Chaudret, *ChemCatChem* 2013, **6**, 87. c) M. Axet, S. Conejero and I.C. Gerber, *ACS Appl. Nano Mater.,* 2018, **1**, 5885.

27 a) P. Tegeder, M. Freitag, K. M. Chepiga, S. Muratsugu, N. Möller, S. Lamping, M. Tada, F. Glorius and B. J. Ravoo, *Chem. Eur. J.*, 2018, **24**, 18682. b) R. Ye, A. V. Zhukhovitskiy, R. V. Kazantsev, S. C. Fakra, B. B. Wickemeyer, F. D. Toste and G. A. Somorjai, *J. Am. Chem. Soc.*, 2018, **140**, 4144.

28 J. B. Ernst, S. Muratsugu, F. Wang, M. Tada and F. Glorius, *J. Am. Chem. Soc.*, 2016, **138**, 10718.

29 A. Palazzolo, T. Naret, M. Daniel-Bertrand, D. Buisson, S. Tricard, P. Lesot, Y. Coppel, B. Chaudret, S. Feuillastre and G. Pieters, *Angew. Chem.*, 2020, **132**, 21065.

30 a) D. Ventura-Espinosa, S. Martín, H. García and J. A. Mata, *J. Catal.*, 2021, **394**, 113. b) D. Ventura-Espinosa, S. Martín and J. A. Mata, *J. Catal.*, 2019, **375**, 419. c) A. Mollar-Cuni, D. Ventura-Espinosa, S. Martín, Á. Mayoral, P. Borja and J. A. Mata, *ACS Omega* 2018, **3**, 15217.

31 a) L. M. Martínez-Prieto, M. Puche, C. Cerezo-Navarrete and B. Chaudret, *J. Catal.*, 2019, **377**, 429. b) b) C. Cerezo-Navarrete, Y. Mathieu, M. Puche, C. Morales, P. Concepción, L. M. Martínez-Prieto and A. Corma, *Catal. Sci. Technol.*, 2021, **11**, 494.

32 D. Ventura-Espinosa, S. Sabater and J. A. Mata, *J. Catal.*, 2017, **352**, 498.

33 S. Stankovich, D. A. Dikin, R. D. Piner, K. A. Kohlhaas, A. Kleinhammes, Y. Jia, Y. Wu, S. B. T. Nguyen and R. S. Ruoff, *Carbon* 2007, **45**, 1558.

34 a) L. M. Martinez-Prieto, I. Cano, A. Marquez, E. A. Baquero, S. Tricard, L. Cusinato, I. del Rosal, R. Poteau, Y. Coppel, K. Philippot, B. Chaudret, J. Campora and P. W. N. M. van Leeuwen, *Chem. Sci.,* 2017, **8**, 2931.

35 L. M. Martinez-Prieto, C. Urbaneja, P. Palma, J. Campora, K. Philippot and B. Chaudret, *Chem. Commun.,* 2015, **51**, 4647.

36 F. Novio, K. Philippot and B. Chaudret, *Catal. Letters* 2010, **140**, 1.

37 M. Koy, P. Bellotti, M. Das and F. Glorius, *Nat. Catal.*, 2021, **4**, 352.

38 F. Martinez-Espinar, P. Blondeau, P. Nolis, B. Chaudret, C. Claver, S. Castillón and C. Godard, *J. Catal.*, 2017, **354**, 113.

39 A. Rühling, K. Schaepe, L. Rakers, B. Vonhören, P. Tegeder, B. J. Ravoo and F. Glorius, *Angew. Chem. Int. Ed.,* 2016, **55**, 5856.

40 P. W. N. M. van Leeuwen, *Homogeneous Catalysis-Understanding the Art*, Kluwer Academic Publishers, Netherlands, 2004.

41 a) A. Denicourt-Nowicki, B. Leger and A. Roucoux, *Phys. Chem. Chem. Phys.*, 2011, **13**, 13510. b) D. Duraczynska, A. Drelinkiewicz, E. Bielanska, E. M. Serwicka and L. Litynska-Dobrzynska, *Catal. Lett.*, 2011, **141**, 83.

42 M. Yang, G. Cheng, D. Xie, T. Zhu, Y. Dong, H. Ke and H. Cheng, *Int. J. Hydrogen Energy* 2018, **43**, 8868.